A Dual Modular Multilevel Converter with High-Frequency Circulating Current Injection for MV Open-End Stator Winding Machine Drives

Mohamed S. Diab[1], Xibo Yuan[1], and Barry W. Williams[2]
[1]*Department of Electrical and Electronic Engineering, University of Bristol, Bristol, United Kingdom*
[2]*Department of Electrical and Electronic Engineering, University of Strathclyde, Glasgow, United Kingdom*

Abstract—**Since its emergence in 2002, the modular multilevel converter (MMC) has been extensively addressed as a promising candidate for medium-voltage machine drives. However, the MMC application as a variable-speed drive experiences a serious challenge pertinent to its unique operating principles, resulting in wide voltage fluctuations across the MMC floating capacitors inversely proportional to the operating frequency. The high-frequency circulating current injection is the mainstream approach to suppress the capacitor voltage ripple at lower operating frequencies, however at the expense of introducing high-frequency common-mode voltage at the machine terminals. This paper adopts the high-frequency circulating current injection approach in a dual MMC topology applicable to open-winding machine drives, with the advantage of mitigating the high-frequency common-mode voltage at the machine terminals by exploiting an inherent feature in open-winding configurations. The theoretical analysis of common-mode voltage mitigation is presented in this paper supported with verification results based on MATLAB simulation.**

***Index Terms*—Capacitor voltage ripple, common-mode voltage, high-frequency injection, medium-voltage (MV) drives, modular multilevel converter (MMC), open-winding machines, variable-speed drives.**

I. Introduction

Due to its beneficial attributes, the modular multilevel converter (MMC) has been a proven technology for medium- to high-voltage high-power applications, outperforming its state-of-the-art counterparts [1]. Enjoying an outstanding industrial position, the MMC is currently serving as a standard converter interface in the high-voltage direct-current transmission systems, while recently has put a toe in the medium-voltage (MV) high-power machine drives market.

The low-frequency operation of the MMCs, an essential requirement in variable-speed drives, experiences serious challenges pertinent to their unique operating principles. Due to their floating nature, the MMC submodule (SM) capacitors are directly exposed to load current circulation, resulting in capacitor voltage fluctuations at the fundamental operating frequency. At lower frequencies, the voltage fluctuations increase, reaching extreme levels at near zero frequencies. MMC low-frequency operation becomes even harder with constant torque loads, where the SM capacitor voltage variation further increases due to the increased load current. This precludes the MMC from MV applications with constant Volt/Hertz control, that is, constant torque loads, limiting its utilization to a narrow band of quadratic-torque loads such as pumps, fans, and compressors [2].

Several approaches have been proposed in the literature to restrain the inherent problem of wide voltage fluctuations across the MMC floating capacitors at low operating frequencies. These approaches can be generally classified into software-based [2]-[7] and hardware-based solutions [8]-[13]. Most of these approaches achieve acceptable performance when operating at reduced frequencies, but with unavoidable trade-offs [14].

Among the introduced mitigation approaches in literature, the high-frequency (HF) circulating current injection method has shown clear potential to satisfactorily suppress the SM capacitor voltage ripple at low operating frequencies. Being a software-based solution, the HF injection approach preserves the standard MMC structure without altering its performance characteristics. However, the HF injection approach increases the MMC arm currents, thus increases the current stress of the switching devices, which necessitates oversizing the current capacity of the switching devices with higher cooling requirements. Further, it introduces HF common-mode (CM) voltage at the motor terminals resulting in insulation and bearing current problems that harm the motor and shorten its lifetime [2].

To reduce the injected circulating current peak, the HF injected waveforms were reshaped from a sinusoidal waveform into square and quasi-square waveforms, achieving 50% reduction in MMC peak arm current [15]. To alleviate the CM voltage associated with the HF injection method, a family of modified MMC structures have been proposed in [16]–[19] employing physical power transfer channels between the MMC arms for power redistribution and CM voltage compensation. The additional employed hardware to the standard MMC topology dispossesses the HF injection approach its main merit; being a software-based approach that does not alter the MMC standard structure. This gives a margin for extra research effort to maintain a tolerable ripple range of MMC SM capacitor voltage within the entire speed range of the machine while eliminating the CM voltage at the machine terminals.

This paper suggests applying the HF injection scheme to dual MMC topologies for open-end stator winding machines. Exploiting the out-of-phase modulation of the dual MMC topology, the HF CM voltage at the machine terminals is mitigated while preserving the same number and power rating of employed switching devices and passive components.

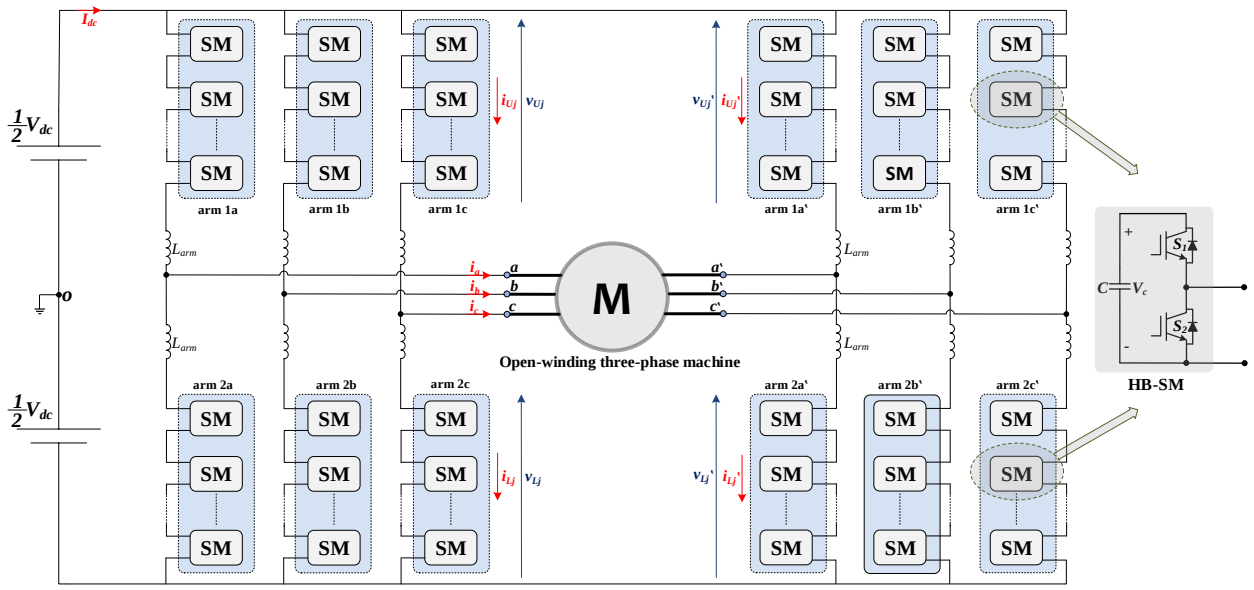

Fig. 1 Dual MMC supplying open-winding machine.

II. Dual MMC Topology for Open-End Stator Winding Machines

For high-power applications, machines with open-end stator windings are considered a possible alternative to conventional star- and delta-connected stators, with the advantages of suppressing the switching CM voltages and improving the output voltage quality [20]. Open-ended machines are supplied through dual inverter configurations that employ two inverters, which enhances the reliability under fault condition at one inverter side. A salient advantage of dual inverter topologies is their ability to achieve the same maximum output voltage-magnitude as the conventional single-sided ones with half of the dc-link voltage, which reduces the insulation requirement. Recently, the dual inverter topology has been realized based on the MMC, offering a single dc-source operation regardless of the number of the output voltage levels, which eliminates bulky and expensive multi-winding isolation transformers to provide isolated dc sources [21], [22]. Further, the dual MMC topology offers more redundant switching state combinations, compared to a single-sided MMC with the same number of output voltage levels, that can be exploited in voltage balancing of the SM capacitors.

A. Structure

The MMC structure is based on series connection of identical SMs, where the SM is the basic building block which lies behind the MMC modularity feature. The circuit diagram of a three-phase dual MMC topology is shown in Fig. 1, comprising two three-phase MMCs each feeding three end-terminals of an open-winding machine, while both MMCs are modulated out-of-phase. Each MMC is composed of three-phase legs each comprising two arms, namely the upper and lower arms. Both arms are connected in series between the dc terminals through arm inductors L_{arm}, while the ac terminal is realized as the intermediary node between the two arms. The arm inductor serves as a current limiter to suppress the circulating current due to the voltage mismatch between the total voltages of the phase legs and the dc-link voltage. Each arm is formed by N series connected SMs, where the number N varies from less than ten up to several hundreds, depending on the application voltage requirements. The SM is a two-terminal circuit incorporating a local capacitor of an equivalent capacitance C and a nominal voltage V_c, acting as an energy buffer to realize the dc voltage source by which the multilevel voltage waveform is synthesized. Each arm is designed to block the full dc-link voltage V_{dc}, yielding the nominal voltage of each SM capacitor $V_c = V_{dc}/N$. The SM can be implemented through several configurations, although the half-bridge (HB) and full-bridge (FB) configurations are the most common.

The dual MMC structure can be considered as a direct consequence of splitting each phase-leg of a conventional single-sided MMC into dual complemented legs each with half the number of SMs, compared to the single-sided phase leg. Thus, for the same amount of power, the total number of SMs employed in a dual MMC topology is the same as the number of SMs in a conventional single-sided topology. Additionally, the voltage and current stress of the SM capacitors and switching devices is identical in both MMC topologies. Although the number of arm inductors is doubled compared to a conventional single-sided MMC topology, as depicted in Fig. 1, the equivalent arm inductance of the dual MMC topology remains the same.

B. Basic Circuit Analysis

Referring to Fig. 1, the mathematical analysis is derived for the two MMC legs, with a common machine winding, that provide the output nodes a and a'. The differential voltage $v_{aa'}$ across the machine winding in addition to the machine phase current i_a are given as:

$$v_{aa'} = V_o \cos(\omega t) \quad (1)$$

$$i_a = I_o \cos(\omega t - \varphi) \quad (2)$$

where V_o and I_o are the voltage and current amplitudes, respectively, ω is the output angular frequency, and φ is the machine power-factor angle. The phase voltage magnitude is defined by the modulation index M and the voltage of the input source V_{dc}, as:

$$V_o = MV_{dc} \quad (3)$$

Since each two MMC legs with a common machine winding have an out-of-phase modulation, the reference voltages for the MMC arms in addition to the arm currents are given by (4)−(6). The subscripts U and L denote the 'upper' and 'lower' arm, respectively, while $i_{cm\,a}$ and $i_{cm\,a'}$ are the CM currents of the two complemented legs in the dual MMC topology and are often referred to as circulating currents.

$$v_{Ua} = v_{La'} = \frac{1}{2}V_{dc} - \frac{1}{2}v_{aa'} \quad (4a)$$

$$v_{La} = v_{Ua'} = \frac{1}{2}V_{dc} + \frac{1}{2}v_{aa'} \quad (4b)$$

$$i_{Ua} = i_{cm\,a} + \frac{1}{2}i_a \quad (5a)$$

$$i_{La} = i_{cm\,a} - \frac{1}{2}i_a \quad (5b)$$

$$i_{Ua'} = i_{cm\,a'} - \frac{1}{2}i_a \quad (6a)$$

$$i_{La'} = i_{cm\,a'} + \frac{1}{2}i_a \quad (6b)$$

C. Arm Ripple Power

Multiplying the arm voltages by corresponding arm currents and rearranging the resultant terms, the instantaneous power in the upper and lower arms can be categorized, as shown in (7), into a CM component, p_{cm}, which alternates in phase in both arms at twice the line frequency, and a differential-mode (DM) component, p_{dm}, which alternates in anti-phase in the upper and lower arms at the fundamental line-frequency [21].

$$p_{Ua} = p_{cm} + p_{dm} \quad (7a)$$

$$p_{La} = p_{cm} - p_{dm} \quad (7b)$$

$$p_{Ua'} = p_{cm} - p_{dm} \quad (7c)$$

$$p_{La'} = p_{cm} + p_{dm} \quad (7d)$$

Due to the dual frequency alternation of the MMC arm power, the SM capacitor voltage fluctuations have CM and DM voltage-ripple components alternating at twice the fundamental frequency and at the fundamental frequency, respectively. In [21], the SM capacitor voltage ripple has been analyzed in detail for a dual MMC topology, showing that the fundamental-frequency DM component is dominant in the SM capacitor voltage ripple. Thus, the DM arm power component should be tightly controlled so that the capacitor voltage-ripple does not exceed tolerated values.

III. HF Circulating Current Injection in Dual MMC Topology

With MMC operation enjoying two degrees of freedom, represented in the CM phase voltage and the circulating current, the HF injection approach implies injecting HF voltage to the converter output phase voltage and HF CM current to the phase-leg circulating current. The coexisted HF injected signals in each MMC arm create HF ripple power that can be used to counterbalance the DM ripple power [23].

Although several waveforms can be adopted as HF injected signals, the square waveforms are considered in the analysis for simplicity. The HF power component (p_h) required to fully counter the DM arm power in (7) can be calculated as:

$$p_h = v_h\, i_h = p_{dm} \quad (8)$$

where i_h is the HF injected square-wave circulating current, while v_h is the superimposed HF square wave CM voltage which is given by (9) with V_h is the magnitude of HF injected

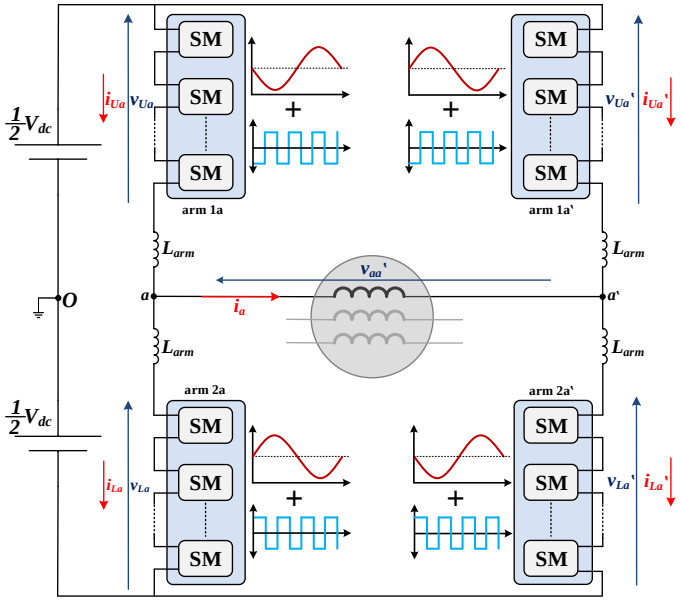

Fig. 2 HF square-wave injection in one of the dual MMC phase-legs.

voltage, f_h is the frequency of injected signals, and $rect(f_h, t)$ is a periodic square wave function as given by (10).

$$v_h = V_h\, rect(f_h, t) \quad (9)$$

$$rect(f_h, t) = \begin{cases} -1 & if\ (0 < t \le \dfrac{1}{2f_h}) \\ 1 & if\ (\dfrac{1}{2f_h} < t \le \dfrac{1}{f_h}) \end{cases} \quad (10)$$

Substituting (9) and (10) in (8), the injected HF circulating current is:

$$i_h = \frac{p_{dm}}{V_h}\, rect(f_h, t) \quad (11)$$

Typically, to avoid unnecessary increase in current stress and power loss of the switching devices, the injected circulating current is recommended to be minimized, however at the expense of increased magnitude of the injected HF voltage, as indicated in (11). This increases the resultant CM voltage at the machine terminals deteriorating the machine performance and degrading its lifetime.

Generally, the CM voltage, v_{cm}, of a single-sided inverter is calculated as the average of the three-phase output voltages measured with respect to the ground point. For a dual-sided inverter, two CM voltages (v_{cm1} and v_{cm2}) are calculated for each individual inverter, where the net CM voltage is the difference between them. Referring to Fig. 1, the net CM voltage for the open-winding machine is calculated as:

$$\begin{aligned} v_{cm} &= v_{cm1} - v_{cm2} \\ &= \tfrac{1}{3}(v_{ao} + v_{bo} + v_{co}) - \tfrac{1}{3}(v_{a'o} + v_{b'o} + v_{c'o}) \end{aligned} \quad (12)$$

A. Mitigation of CM Voltage

With the advantageous attribute of open-winding machines being supplied from two inverters modulated out-of-phase, the HF injection approach can be adopted while mitigating the HF CM voltage at the machine terminals. This is elucidated in Fig. 2, where the dual MMC phase-legs that provide the output nodes a and a' are shown under HF injection using

square-wave signals. The upper and lower arms of each MMC leg have out-of-phase HF CM square-wave voltages such that the total voltage across the MMC leg is V_{dc}. However, each two adjacent MMC arms with a common machine winding have in-phase HF CM square-wave voltages. This results in the CM voltage of the left-side MMC (v_{cm1}) be countered by the CM voltage of the right-side MMC (v_{cm2}), as depicted in (12), resulting in a zero net CM voltage at the machine terminals.

B. HF Injection Control Algorithm

The HF signals are deliberately injected into the MMC arms by controlling the waveform of both v_{cm} and i_{cm}, without affecting neither the output voltage nor current. When the HF voltage, v_h, is added to the converter output phase voltage and the HF CM current, i_h, is added to the circulating current, new arm voltages and currents are obtained as given by (13)−(16) for the dual MMC leg providing the output nodes a and a'.

$$v_{Ua} = \frac{1}{2}V_{dc} - \frac{1}{2}v_{aa'} - v_h \quad (13a)$$

$$v_{La} = \frac{1}{2}V_{dc} + \frac{1}{2}v_{aa'} + v_h \quad (13b)$$

$$v_{Ua'} = \frac{1}{2}V_{dc} + \frac{1}{2}v_{aa'} - v_h \quad (14a)$$

$$v_{La'} = \frac{1}{2}V_{dc} - \frac{1}{2}v_{aa'} + v_h \quad (14b)$$

$$i_{Ua} = i_{cm\,a} + \frac{1}{2}i_a + i_h \quad (15a)$$

$$i_{La} = i_{cm\,a} - \frac{1}{2}i_a + i_h \quad (15b)$$

$$i_{Ua'} = i_{cm\,a'} - \frac{1}{2}i_a + i_h \quad (16a)$$

$$i_{La'} = i_{cm\,a'} + \frac{1}{2}i_a + i_h \quad (16b)$$

To reduce the power loss in the switching devices, the magnitude of the injected HF circulating current should be minimized by increasing the magnitude of the HF injected voltage. Since the CM voltage is mitigated at the open-winding machine terminals, the magnitude of the HF injected voltage can be maximized without overmodulation, as:

$$V_h = \frac{1}{2}V_{dc}(M_{max} - M) \quad (17)$$

where M_{max} is the maximum MMC modulation index at the rated operating frequency f_r. With constant Volt/Hertz control, the modulation index is defined according to the following relationship:

$$M = \frac{\omega}{\omega_r}M_{max} \quad (18)$$

where ω is the angular speed at a frequency f, while ω_r is the rated angular speed at the rated frequency f_r.

Traditional HF injection methods fully compensate the DM ripple power by the deliberately created HF power. However, this results in unnecessarily higher circulating current magnitude and power losses. Alternatively, an improved HF circulating current injection method is adopted in this paper as suggested in [25], which maintains the SM capacitor voltage ripple within reasonable limits throughout the entire frequency range. Since the SM capacitor voltage ripple increases as the operating frequency decreases, the control algorithm increases the magnitude of the HF injected circulating current inversely with the operating frequency. A pre-defined speed limit ω_{lim} is used to decide when to inject the HF signals. That is, if

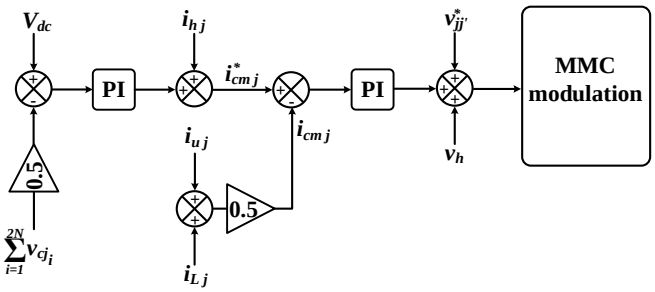

Fig. 3 Control block diagram of HF injection method.

$\omega > \omega_{lim}$, no HF power is created where the SM capacitor voltage ripple is assumed to be within the tolerable range. However, when $\omega < \omega_{lim}$, the required HF power is set to limit the SM capacitor voltage ripple within tolerated values. Accordingly, the HF CM injected current, for leg a, is given as [24]:

$$i_{ha} = \frac{(1 - \omega/\omega_{lim})i_a}{2M_{max}(1 - \omega/\omega_{lim})}rect(f_h, t) \quad (19)$$

A control block diagram elaborating the HF injection scheme, for a general MMC phase-leg j, is presented in Fig. 3. Although the HF voltage injection is directly realized through MMC modulation, the CM current injection implies tracking control which imposes limitations on the bandwidth of the current control loop. To achieve good controllability of the injected current, the choice of f_h must be less than $1/10$ the MMC switching frequency. Whereas, to satisfactorily mitigate the SM capacitor voltage ripple at low-operating frequencies, f_h is recommended to be at least 4–10 times the mid-range operating frequency [25]. Thus, for a 50 Hz rated frequency, i.e. $f_r = 50$ Hz, the injected signals are maintained at 100–250 Hz.

C. MMC Control

Each MMC phase-leg is controlled by a modulator that commands a varying number of SMs to be inserted at each time instant according to a phase disposition PWM scheme. Each modulator operates according to a sinusoidal reference input signal with an HF injected voltage which depends on the operating frequency. The SM capacitor voltage balancing is maintained by a selection mechanism based on capacitor voltage measurements at each switching instant. This mechanism sorts the SM capacitor voltages and then decides which individual SM be inserted or bypassed, according to the arm current direction [26].

IV. VERIFICATION

The performance of the dual MMC topology under HF circulating current injection is examined using a 0.75-MW MATLAB/SIMULINK model. The simulations are performed at different operating frequencies where the steady-state operation of the dual MMC is shown at 50 Hz, 25 Hz, and 10 Hz. The simulation parameters are listed in Table I, while the simulation results are shown in Figs. 4−6.

Fig. 4 shows the fundamental waveforms of the dual MMC topology at 50 Hz when feeding a three-phase *RL* load *(R*=40Ω and *L*=50mH*)* connected in an open-end configuration via three-paralleled dual legs, each with five SMs per arm, supplied from a 5-kV dc input voltage. The speed limit after which the

TABLE I
PARAMETERS FOR SIMULATION

Number of SMs per arm (N)	5
Rated active power	0.75 MW
Input dc voltage (V_{dc})	5 kV
Rated current magnitude (I_o)	100 A
Maximum modulation index (M_{max})	0.9
Nominal SM capacitor voltage (V_c)	1 kV
Rated output frequency (f_r)	50 Hz
Injection frequency (f_h)	250 Hz
Carrier frequency of MMC (f_c)	2 kHz
Arm inductance (L_{arm})	3 mH
SM capacitance (C)	1.8 mF

HF injection approach is activated is set at a frequency $f_{lim} = 40$ Hz. That is, the simulation results in Fig. 4 are obtained with traditional MMC control, i.e. without HF injection, where the modulation index equals the maximum modulation index given in Table I. The differential output voltages across the terminals of the open-end load traverse in eleven voltage steps. The three-phase load currents are shown with high-quality sinusoidal profile with rated current magnitude, i.e. $I_o = 100$ A. The arm voltages of phase-leg a are shown unipolar, since HB SMs are used, with sinusoidal modulation. The arm currents are sinusoidal and anti-phase, resulting in a nearly constant CM current. Samples of the SM capacitor voltages in the upper and lower arms are shown balanced with limited voltage ripple (<±10%), where the nominal SM capacitor voltage is 1 kV. The CM voltage of dual-sided MMC is measured as given by (12), where it is shown bounded within ±0.5 kV.

Figs. 5 and 6 show the performance of the dual MMC topology at 25 Hz and 10 Hz, respectively, according to a Volt/Hertz control scheme. In this scenario, the output voltage is reduced in accordance to the operating frequency reduction, while the load resistance is varied linearly with the operating frequency to maintain the output current constant at the rated value to emulate the constant torque characteristic of variable-speed motors. Since the operating frequencies are lower than f_{lim}, the HF injection algorithm is activated as presented in Fig. 3. Common to Figs. 5 and 6, the three-phase output voltages traverse in lower voltage levels compared to their counterparts in Fig. 4. This returns to the reduction in the modulation index at lower operating frequencies, as given by (18). However, the load currents are maintained sinusoidal at the rated current magnitude. The arm voltages have sinusoidal and HF square-wave components due to the injection of HF voltage in the output CM voltage. Likewise, the arm currents have anti-phase sinusoidal components in addition to in-phase HF square-wave CM current as generated by (19). This results in the circulating current alternating at f_h, allowing the SM capacitors to be charged and discharged more frequently such that their voltage ripple is attenuated. This is depicted in the shown samples of the SM capacitor voltages in the upper and lower arms, where the voltage ripple is limited to ±10% despite operating at reduced frequencies. Although HF voltage signals are injected in the phase voltages as a CM voltage, they are counterbalanced in the net CM voltage at the load terminals, where similar to the CM voltage obtained in Fig. 4 without HF injection, the CM voltage in Figs. 5 and 6 are bounded within ±0.5 kV.

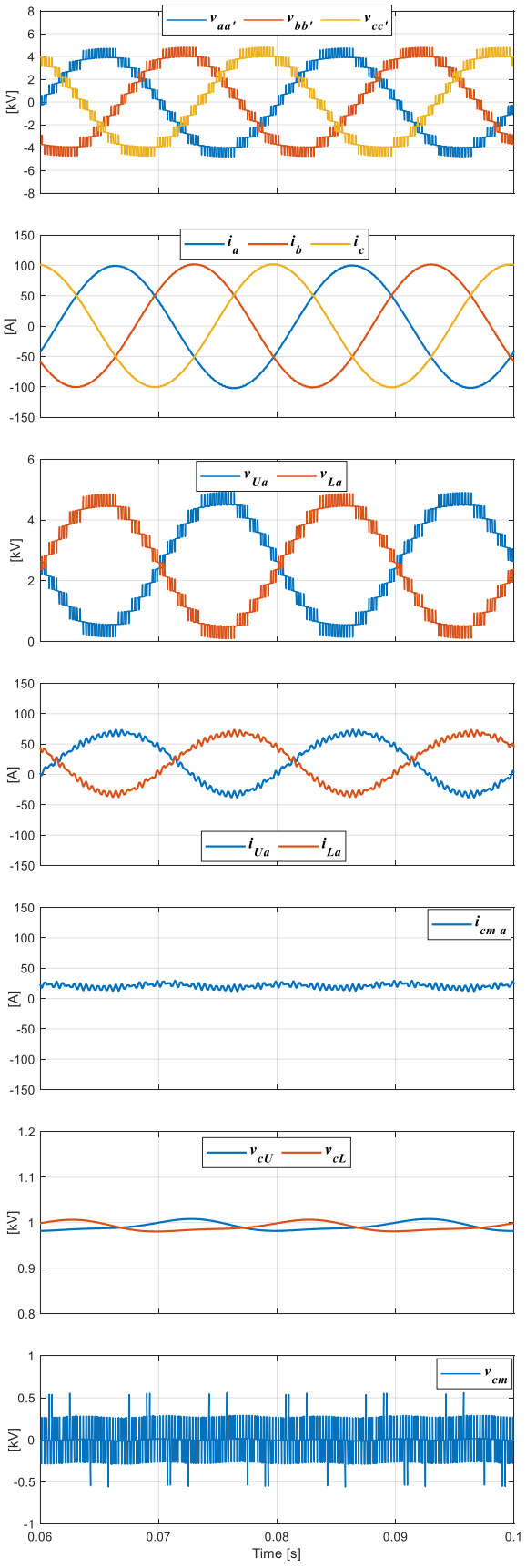

Fig. 4 Simulation waveforms for a steady-state operation of the dual MMC topology at 50 Hz.

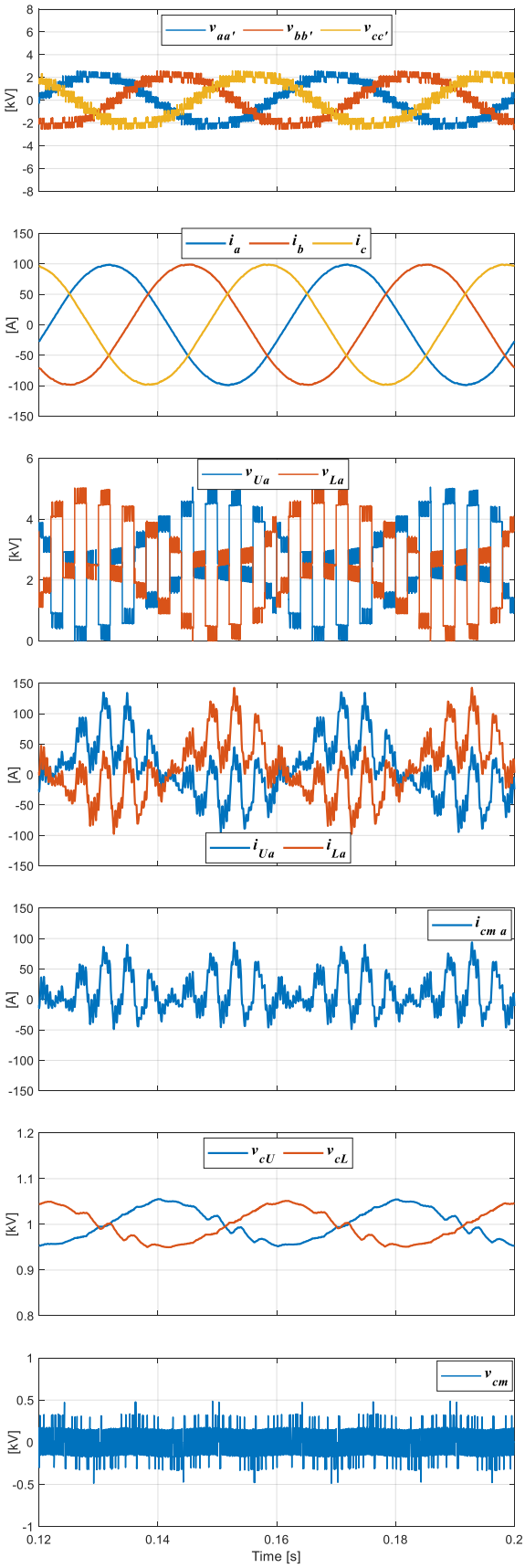

Fig. 5 Simulation waveforms for a steady-state operation of the dual MMC topology at 25 Hz using the HF injection approach.

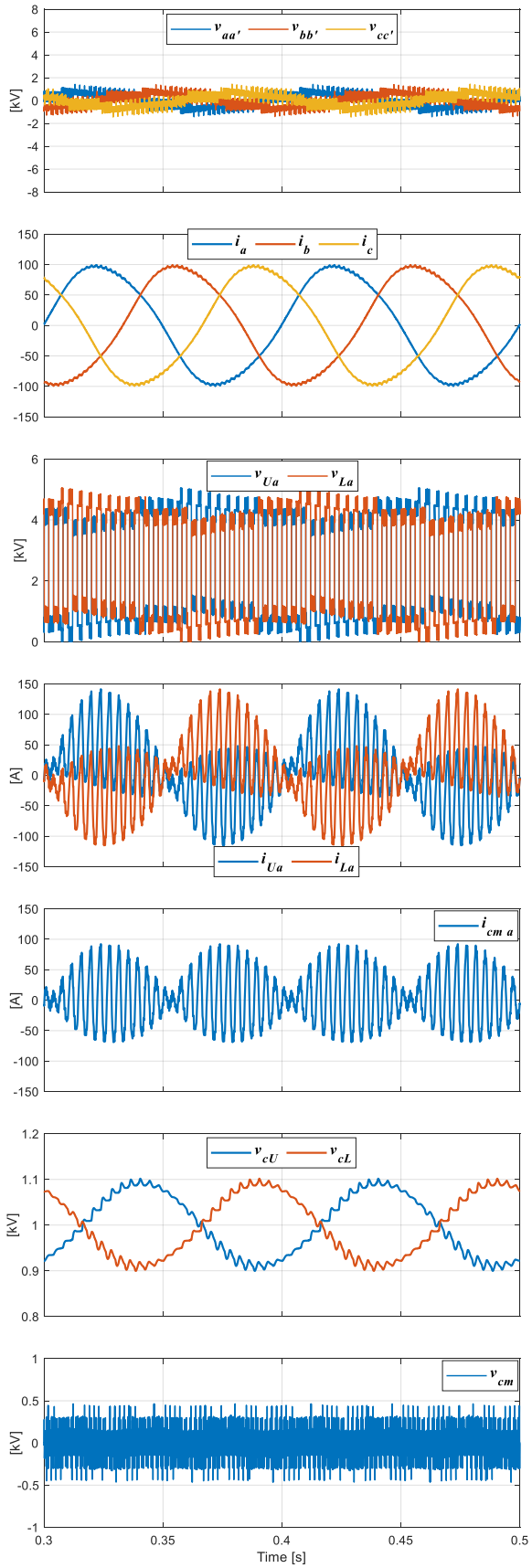

Fig. 6 Simulation waveforms for a steady-state operation of the dual MMC topology at 10 Hz using the HF injection approach.

TABLE II
ASSESSMENT OF THE DUAL MMC TOPOLOGY WITH OTHER ALTERNATIVES UNDER HF INJECTION

	Machine configuration	Ability to mitigate HF CM voltage	Additional hardware	Restrictions on the number of SMs per arm	Notes
Standard MMC Topology	Any machine configuration	×	×	×	It is considered as a reference to compare other topologies
Active Cross Connected MMC [16]	Any machine configuration	✓	$3N$ HB-SMs	must be even number	The number of switching devices is increased by 50%
Flying Capacitor MMC [17]	Any machine configuration	✓	3 flying capacitors	must be even number	The flying capacitors need pre charging and are rated at half the dc-link voltage
Star-Channel MMC [18]	Any machine configuration	✓	$0.75N$ FB-SMs	must be even number	The number of switching devices is increased by 25%
Delta-Channel MMC [19]	Any machine configuration	✓	$0.75\sqrt{3}N$ FB-SMs	must be even number	The number of switching devices is increased by 43%
Dual MMC Topology	Open-end winding machines	✓	×	×	It achieves 50% reduction in required dc-link voltage.

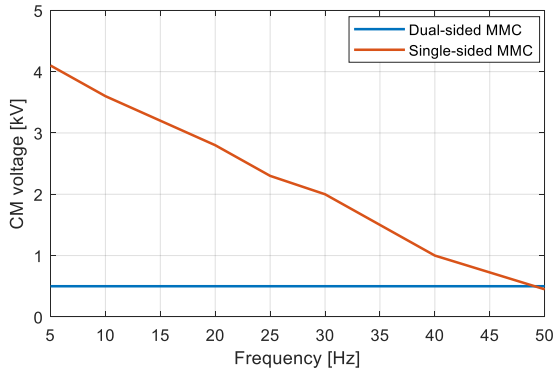

Fig. 7 CM voltage variation with operating frequency under HF injection approach using single-sided and dual-sided MMCs.

It should be noted that the dual MMC topology cannot achieve zero CM voltage. This is due to the imbalance between the voltages of each three-phase set, where it is impossible to make the sum of three output voltages instantaneously equal to zero with PWM switched output levels, however, this sum can be reduced by increasing the number of voltage levels.

Fig. 7 shows the variation of the CM voltage with the operating frequency under the HF injection approach using the conventional single-sided MMC and the dual MMC. Common to both topologies, the magnitude of the HF injected CM voltage increases as the operating frequency decreases to attenuate the SM capacitor voltage ripple. However, the net CM voltage of the dual MMC is almost constant at 0.5 kV regardless of the operating frequency, where the injected HF CM voltages are counterbalanced. Oppositely, the net CM voltage of the single-sided MMC is inversely proportional to the operating frequency.

V. ASSESSMENT

Table II highlights the features of the dual MMC topology under HF injection approach compared to the single-sided MMC topologies proposed in [16]–[19], that employ extra hardware to mitigate the HF CM voltage. It can be shown that the dual MMC preserves the same hardware and performance of the single-sided MMC, however with the ability to mitigate the HF CM voltage. It also generates the same output voltage magnitude as the single-sided MMC using half the dc-link voltage at the same power rating of the switching devices. Only the number of generated voltage levels are halved in the dual MMC compared to an equivalently rated single-sided MMC. However, this does not affect the quality of the output current when the number of employed SMs is relatively high.

Other alternative topologies based on single-sided MMC adopt extra hardware to mitigate the HF CM voltage by dividing each MMC arm into two sub-arms while their conjunction nodes are drawn out to connect the middle taps of each pair of upper and lower arms through a cross-connected branch. The branch has been realized through either N HB-SMs or a flying capacitor, yielding an active cross-connected MMC [16] and a flying capacitor MMC [17]. Likewise, in [18] and [19], each arm is divided into two halves, with cross connection of each set of three adjacent arms at their middle tap nodes through two sets of star-/delta-channel branches yielding star channel MMC and delta channel MMC, respectively. Common to both topologies, the star/delta channels are realized through a series connection of FB SMs. The pros and cons of these single-sided-based MMC topologies are highlighted in Table II.

VI. CONCLUSION

This paper has suggested applying the HF circulating current injection approach to a dual MMC topology applicable to open-winding MV machine drives, to suppress the SM capacitor voltage ripple at reduced operating frequencies while mitigating the associated HF CM voltage at the machine terminals based on inherent feature of open-winding configurations. The hardware required to implement the dual MMC topology is the same as that employed in an equivalently rated single-sided MMC, with the advantage of operating at half the dc-link voltage to generate the same output voltage magnitude. The performance of the dual MMC topology has been assessed under HF injection using MATLAB simulation at different operating frequencies. The obtained results validated the theoretical analysis of SM capacitor voltage ripple suppression and CM voltage mitigation. Unlike the single-sided MMC topologies that apply extra hardware to mitigate the CM voltage under HF injection algorithm, the dual MMC topology preserves the same hardware and performance of the single-sided MMC, however with the ability to mitigate the HF CM voltage.

REFERENCES

[1] A. Lesnicar and R. Marquardt, “An innovative modular multilevel converter topology suitable for a wide power range,” in *Proc. IEEE Power Tech. Conf*., Bologna, Italy, vol. 3, Jun. 23–26, 2003.

[2] A. Korn, M. Winkelnkemper, and P. Steimer, “Low output frequency operation of the modular multi-level converter”, in Proc. IEEE ECCE, 2010, pp. 3993–3997.

[3] A. Antonopoulos, L. Angquist, L. Harnefors, and H. P. Nee, “Optimal selection of the average capacitor voltage for variable-speed drives with modular multilevel converters,” *IEEE Trans. Power Electron.*, vol. 30, no. 1, pp. 227–234, Jan. 2015.

[4] B. Tai, C. Gao, X. Liu, and Z. Chen, “A novel flexible capacitor voltage control strategy for variable-speed drives with modular multilevel converters,” *IEEE Trans. Power Electron*., vol. 32, no. 1, pp. 128–141, Jan. 2017.

[5] R. Yang et al., “Asymmetric mode control of MMC to suppress capacitor voltage ripples in low frequency low voltage condition,” *IEEE Trans. Power Electron.*, vol. 32, no. 6, pp. 4219–4230, Jun. 2017.

[6] M. S. Diab, G. P. Adam, B. W. Williams, A. M. Massoud and S. Ahmed, “Quasi two-level PWM operation of a nine-arm modular multilevel converter for six-phase medium-voltage motor drives,” *2018 IEEE Applied Power Electronics Conference and Exposition* (APEC), San Antonio, TX, 2018, pp. 1641-1648.

[7] A. Mertens and J. Kucka, “Quasi two-level PWM operation of an MMC phase leg with reduced module capacitance,” *IEEE Trans. Power Electron.*, vol. 31, no. 10, pp. 6765–6769, Oct. 2016.

[8] M. S. Diab, B. W. Williams, D. Holliday, A. M. Massoud and S. Ahmed, “A modular multilevel converter with isolated energy-balancing modules for MV drives incorporating symmetrical six-phase machines,” 2017 *IEEE Energy Conversion Congress and Exposition* (ECCE), Cincinnati, OH, USA, 2017, pp. 2715-2722.

[9] L. He, K. Zhang, J. Xiong, S. Fan, X. Chen, and Y. Xue, “New modular multilevel converter with power channels between upper- and lower arms suitable for MV drives,” *IEEE Appl. Power Electron. Conf. Expo*., 2015, Charlotte, NC, USA, pp. 799–805.

[10] M. S. Diab, A. M. Massoud, S. Ahmed and B. W. Williams, "A Modular Multilevel Converter With Ripple-Power Decoupling Channels for Three-Phase MV Adjustable-Speed Drives," *IEEE Trans. Power Electron*., vol. 34, no. 5, pp. 4048-4063, May 2019.

[11] L. He, K. Zhang, J. Xiong, S. Fan, and Y. Xue, “Low-frequency ripple suppression for medium-voltage drives using modular multilevel converter with full-bridge submodules,” *IEEE J. Emerging Sel. Topics Power Electron*., vol. 4, no. 2, pp. 657–667, Jun. 2016.

[12] L. Baruschka, D. Karwatzki, M. von Hofen, and A. Mertens, “Low-speed drive operation of the modular multilevel converter Hexverter down to zero frequency,” in Proc. 2014 IEEE Energy Convers. Congr. Expo., Pittsburgh, PA, USA, 2014, pp. 5407–5414.

[13] B. Li, S. Zhou, D. Xu, S. J. Finney, and B. W. Williams, “A hybrid modular multilevel converter for medium-voltage variable-speed motor drives,” *IEEE Trans. Power Electron*., vol. 32, no. 6, pp. 4619–4630, Jun. 2017.

[14] M. S. Diab, “Modular multilevel converter designs for medium-voltage machine drives,” Ph.D. dissertation, Dept. Electron. Elect. Eng., Univ. Strathclyde, Glasgow, Scotland, 2019.

[15] S. Song, J. Liu, S. Ouyang and X. Chen, “An improved high-frequency common-mode voltage injection method in modular multilevel converter in motor drive application,” *2018 IEEE Applied Power Electronics Conference and Exposition (APEC)*, San Antonio, TX, 2018, pp. 2496-2500.

[16] S. Du, B. Wu, K. Tian, N. R. Zargari and Z. Cheng, “An Active Cross-Connected Modular Multilevel Converter (AC-MMC) for a Medium-Voltage Motor Drive,” *IEEE Trans. Ind. Electron*, vol. 63, no. 8, pp. 4707-4717, Aug. 2016.

[17] S. Du, B. Wu, N. R. Zargari and Z. Cheng, “A Flying-Capacitor Modular Multilevel Converter for Medium-Voltage Motor Drive,” *IEEE Trans. Power Electron.*, vol. 32, no. 3, pp. 2081-2089, March 2017.

[18] S. Du, B. Wu and N. R. Zargari, “A Star-Channel Modular Multilevel Converter for Zero/Low-Fundamental-Frequency Operation Without Injecting Common-Mode Voltage,” *IEEE Trans. Power Electron.*, vol. 33, no. 4, pp. 2857-2865, April 2018.

[19] S. Du, B. Wu and N. R. Zargari, “A Delta-Channel Modular Multilevel Converter for Zero/Low-Fundamental-Frequency Operation,” *IEEE Trans. Ind. Electron.*, vol. 66, no. 3, pp. 2227-2235, March 2019.

[20] M. R. Baiju, K. K. Mohapatra, R. S. Kanchan, and K. Gopakumar, “A dual two-level inverter scheme with common mode voltage elimination for an induction motor drive,” *IEEE Trans. Power Electron*., vol. 19, no. 3, pp. 794–805, May 2004.

[21] M. S. Diab, A. M. Massoud, S. Ahmed and B. W. Williams, "A Dual Modular Multilevel Converter With High-Frequency Magnetic Links Between Submodules for MV Open-End Stator Winding Machine Drives," *IEEE Trans. Power Electron.*, vol. 33, no. 6, pp. 5142-5159, June 2018.

[22] M. S. Diab, A. M. Massoud, S. Ahmed, and B. W. Williams, ‘‘Dual modular multilevel converter with shared capacitor sub-module for MV open-end stator winding machine drives,’’ J. Eng., vol. 2019, no. 17, pp. 4401–4405, Jun. 2019.

[23] A. Antonopoulos, L. Ängquist, S. Norrga, K. Ilves, L. Harnefors, H.-P. Nee, “Modular multilevel converter AC motor drives with constant torque from zero to nominal speed,” *IEEE Trans. Ind. Appl.*, vol. 50, no. 3, pp. 1982-1993, May/Jun. 2014.

[24] B. Li *et al*., "An Improved Circulating Current Injection Method for Modular Multilevel Converters in Variable-Speed Drives," *IEEE Trans. Ind. Electron.*, vol. 63, no. 11, pp. 7215-7225, Nov. 2016.

[25] M. Hagiwara, I. Hasegawa and H. Akagi, “Start-Up and Low-Speed Operation of an Electric Motor Driven by a Modular Multilevel Cascade Inverter,” *IEEE Trans. Ind. Appl.*, vol. 49, no. 4, pp. 1556-1565, July-Aug. 2013.

[26] A. Antonopoulos, L. Angquist, and H.-P. Nee, “On dynamics and voltage control of the modular multilevel converter,” in *Proc. 13th Eur. Conf. Power Electron. Appl.*, Barcelona, Spain, 2009, pp. 1–10.